ANTA 504: Supervised Project

The Interplay of Gaseous Chemical Species and the extent of the Ozone Hole

Phil Emnet

58212711

Supervisor

Adrian McDonald

1 Introduction:

Ozone hole formation over Antarctica during the southern hemisphere spring depends strongly on the presence of polar stratospheric clouds (PSCs) during the Antarctic winter, which in turn depend strongly on the temperature of the stratosphere[1]. PSCs act as heterogeneous catalysts that mediate the conversion of chlorine reservoir species such as HCl and $ClONO_2$ into active chlorine species such as ClO [2]. They also facilitate the removal of NO_x by conversion into HNO_3 and subsequent incorporation into PSC ice crystals [2]. The latter process is called denitrification, and is the main factor in the extent of ozone destruction, as NO_x species convert active chlorine back into inactive forms. Permanent removal of HNO_3 can occur if the ice crystals become heavy enough for sedimentation [2]. As the sun returns in spring, ClO is converted into Cl via photolysis and ozone destruction commences. As the sun's activity increases the PSC ice crystals begin to melt and release HNO_3, which is converted into NO_2 via photolysis which converts the Cl species back to inactive forms [2]. As the atmosphere keeps on warming the polar vortex collapses, bringing ozone levels back to normal by November as ozone rich air from the tropics can now mix with the ozone depleted air [3].

Three types of PSCs are currently known to exist [4]. Type 1a is composed of a solid phase nitric acid trihydrate (NAT), Type 1b is a supercooled ternary solution (STS) made up of H_2O, HNO_3, and H_2SO_4, and Type 2 consists mostly of ice. The work by Hanson and Mauersberger [5] showed that while NAT nucleation occurs at temperatures about 7K above the ice frost point (188K), depending on vapour pressures of H_2O and HNO_3, it does not occur directly after crossing the NAT formation temperature threshold, T_{NAT}. Other work shows that nucleation occurs after average temperatures are below T_{NAT} for a period of several days [6], or after a sudden drop in temperature to the ice point which forms ice crystals that allow heterogeneous NAT nucleation [7]. More recently another process of nucleation has been found to exist, one that only requires short periods of

temperatures below T_{NAT} [8]. However the mechanism of this process is still not understood.

Satellites have been observing the ozone hole since 1978, measuring parameters such as temperature, PSC area, and the concentrations of various chemical species such as H_2O, HNO_3, HCl, and ClO, important factors contributing to the level of ozone destruction. HNO_3 mixing ratios are controlled by meteorological conditions (strength of adiabatic descent, permeability of polar vortex, extent and duration of low temperatures) which create large interannual variability of PSC formation and area, particularly in the Arctic, which also experiences ozone depletion. The difference in severity of PSC formation leads to different HNO_3 depletion patterns, most extreme in Antarctica where PSCs readily form, and more localized and transient in the Arctic where PSCs are harder to form[3]. The small degree of denitrification in the Arctic is not only due to the lack of temperatures below the water ice frost point (188K) but also the lack of temperatures persistently below 192K [9]. There is a strong correlation between the area of gas-phase HNO_3 loss and the area of temperatures below 192K, but a weak correlation between the area of gas-phase HNO_3 loss and the area of temperatures below 195K[9].

This study uses EOS Microwave Limb Sounder (MLS) data between the years of 2005 and 2008 to further investigate the role of temperature in the stratosphere, and to observe the patterns of accumulation and depletion of the various atmospheric chemical species in relation to PSC formation and temperature.

Because of temperature's profound effect on PSC formation there is significant interest in the derivation of PSC area from simple temperature data collected before satellite observations began. This would then enable scientists to approximate the ozone hole extent before satellite observations began, and hence determine when the ozone hole first appeared. This has important implications to restoring the ozone layer, as it will provide a pre-CFC value of ozone levels deemed 'natural' and to which level the present ozone level must rise again before the ozone hole is considered recovered. This natural value would replace the current value, the ozone concentration observed in 1978 by the first satellite.

2 Dataset and Methodology

The Aura satellite which carries the EOS MLS instrument has been in operation since 2004 and has collected data on temperature, BrO, CH_3CN, ClO, CO, H_2O, HCl, HCN, HNO_3, HO_2, HOCl, N_2O, O_3, OH, and SO_2. At the time of study data up to late September 2008 was available, which prevented some of the study due to an incomplete dataset for 2008. MATLAB 7.6.0 was used for data analysis and could read the MLS data directly. In the uncorrected dataset HNO_3 concentrations were overestimated by the satellite at some levels of the stratosphere because two vibrational states of HNO_3 were omitted in the measurements and were significant[10]. An empirical correction has been derived however[11], and the corrected dataset is used for this study. Data on temperature, H_2O, HNO_3, ClO, and HCl were extracted for each pressure level between 13 and 20 (100hPa – **XXX**)

H_2O and HNO_3 concentrations for each pressure level were entered as variables into the phase diagram equations derived by Hanson and Mauersberger [5] to calculate theoretical NAT formation temperatures, T_{NAT}. These were then compared to observed temperatures, and also to the concentrations of the various chemicals. T_{NAT} and observed temperatures were also averaged over certain times of the year, and compared to PSC areas from a different dataset. These PSC areas were calculated by assuming average values of H_2O and HNO_3 concentrations rather than using MLS values (3 ppmv for water, 10 ppbv for nitric acid).

3 Results

3.1 Temperature relationships

When plotting T_{NAT} against observed temperature for any year and pressure level the observed temperature dips below T_{NAT} between around day 170 (mid-late May) and day 270 (early September) plus or minus a few days in May and plus or minus approximately 10 days in September (see Figure1). This time period will be referred to as the T_{NAT} period.

The different variability may be due to seasonal meteorological events, the first temperature crossing being less prone to external influences than the second. This is a month before the official polar vortex period (AVP) begins; from day 199 (18th July) to day 333 (30th November)[12]. T_{NAT} lies around the 195K mark; the standard average temperature NASA uses for its atmospheric calculations. However T_{NAT} dips below 190K for all years at pressure level 17 and above (see Figure 2).

T_{NAT} shows a very strong correlation with water vapour concentrations for every year

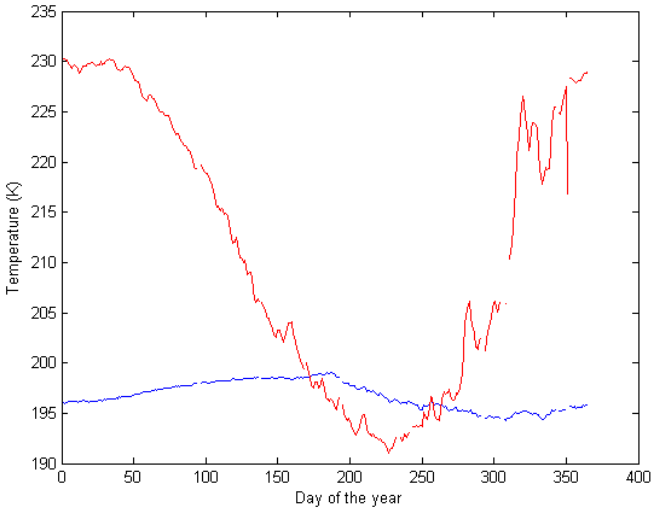

Figure 1: T_{NAT} (blue, K) and observed temperature (red, K) in 2005, Pressure Level 13

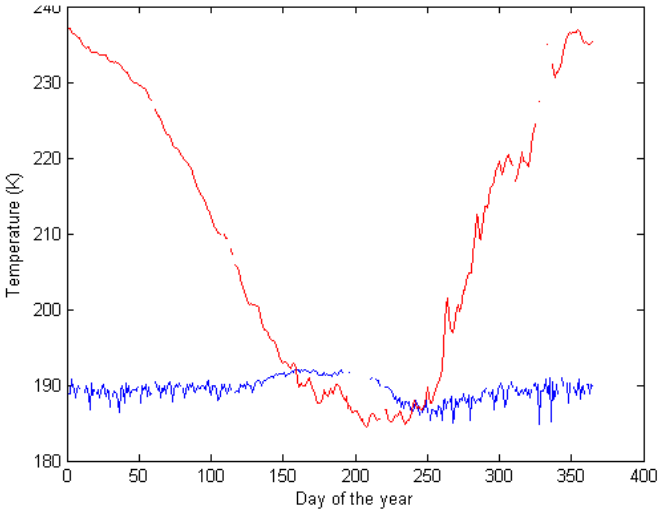

Figure 2: T_{NAT} (blue, K) and observed temperature (red, K) in 2005, Pressure Level 17

observed for pressure levels 13-15 (see Figure 3). The peak in water vapour observed at day 170 before the strong drop is observed in every year for the pressure levels 13-19 and correlates well with T_{NAT} variability. Day 170 coincides with T_{NAT} falling below the observed temperature (Figure 1) which may be the trigger for the water vapour peak. The peak may also be a side effect of another unidentified event The increase may also be due to the rapid adiabatic descent of air from the mesosphere, which is qualitatively consistent with such an event [13]. If this is correct this may be a potential way to measure the descent of air in the Antarctic stratosphere, which may also correlate strongly with O_3 depletion later in the season.

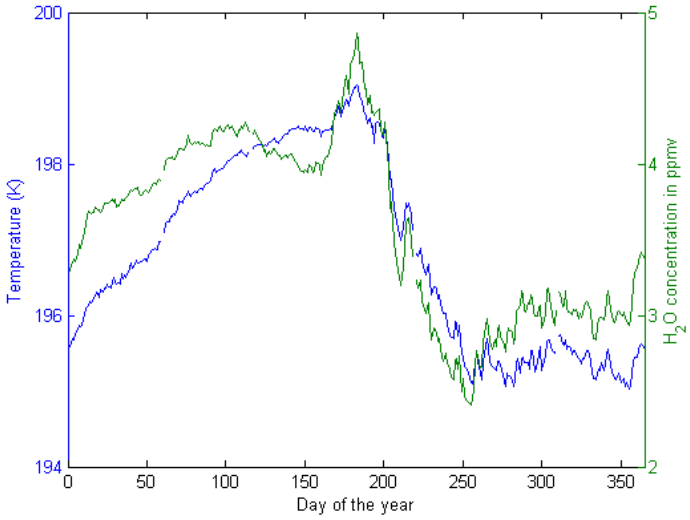

Figure 3: T_{NAT} (blue, K) and H2O concentration (green, ppmv) in 2007, Pressure Level 13

As temperatures drop below T_{NAT} PSCs begin to form, and water vapour concentrations decrease, reaching a minimum at day 250 when temperatures begin to warm again and water vapour increase back to normal, as shown in Figure 1. However this strong T_{NAT}/water correlation begins to break down at pressure level 16 and above (see Figure 4), after which the HNO3 concentrations explain most of the T_{NAT} trend (see Figure 5), though not as well as water vapour did in the lower pressure levels. Water vapour still explains the T_{NAT} trend after day 250, when both begin to rise, whereas HNO_3 levels remain steady during that period.

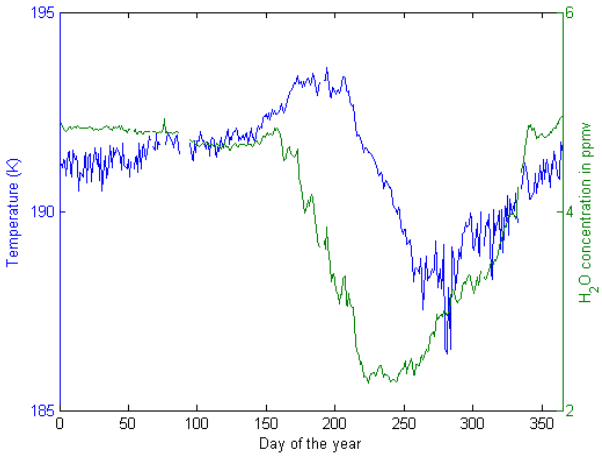

Figure 4: T_{NAT} (blue, K) and H2O concentration (green, ppmv) in 2006, Pressure Level 16

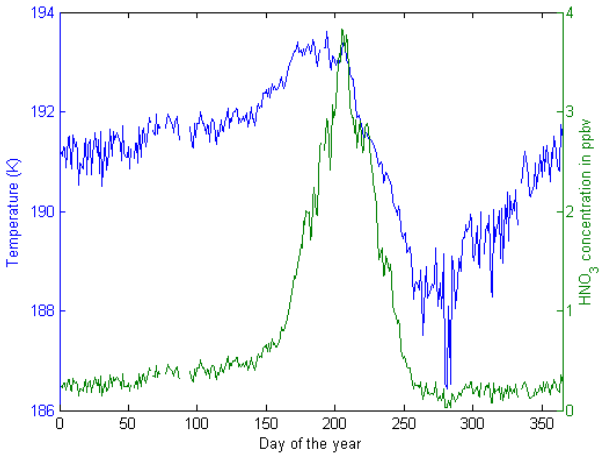

Figure 5: T_{NAT} (blue, K) and HNO3 concentration (green, ppbv) in 2006, Pressure Level 16

3.2 T_{NAT} vs. PSC area

PSC area data was averaged over the AVP and the T_{NAT} period to determine during which period the temperature dependence is greatest.

A very strong non-linear relationship was observed during both monitored periods (see Figures 6-12). This may be because T_{NAT} is an average value over a large area, half the temperatures will be above and half below, which would create some bias and a non-linear relationship may be possible. A relationship during the AVP could not be fully established for 2008 as the available data at the time did not reach until the end of the AVP at day 333.

Figures 6-8 show plots of T_{NAT} vs. PSC area during the AVP, all of which show excellent fits for a squared polynomial (average $R^2 = 0.92$). Figures 9-12 show the same plot but during the T_{NAT} period. They too show a strong squared relationship (average $R^2 = 0.77$), though slightly weaker than in Figures 6-8. This shows that T_{NAT} is a more important parameter during the AVP where periods of temperatures above T_{NAT} were observed and PSCs cannot form.

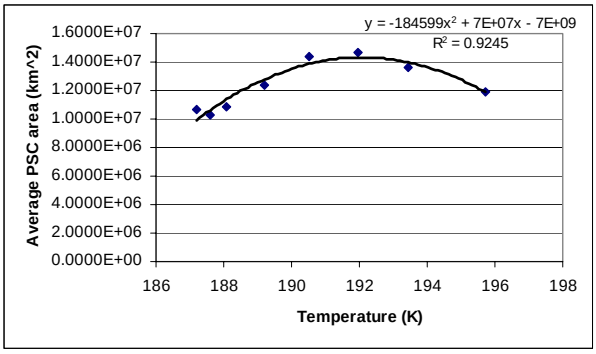

Figure 6: NAT formation temperature (K) vs. average PSC area (km^2) over the AVP for 2005

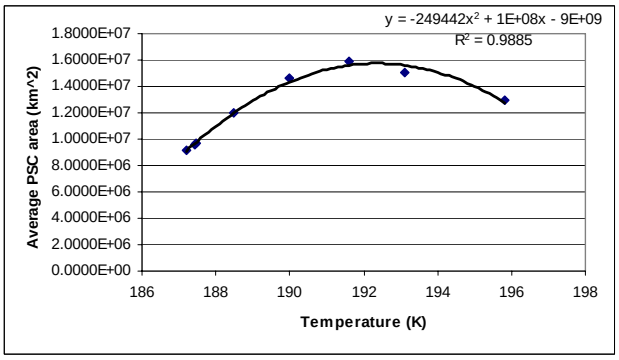

Figure 7: NAT formation temperature (K) vs. average PSC area (km^2) over the AVP for 2006

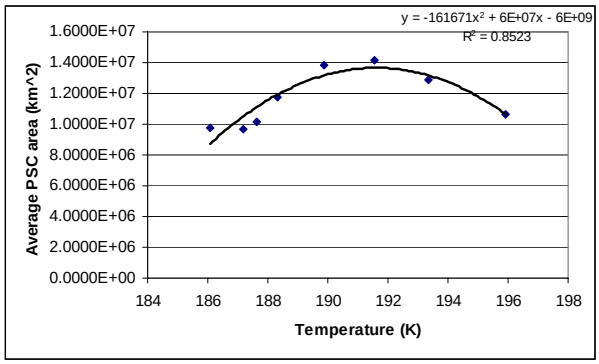

Figure 8: NAT formation temperature (K) vs. average PSC area (km^2) over the AVP for 2007

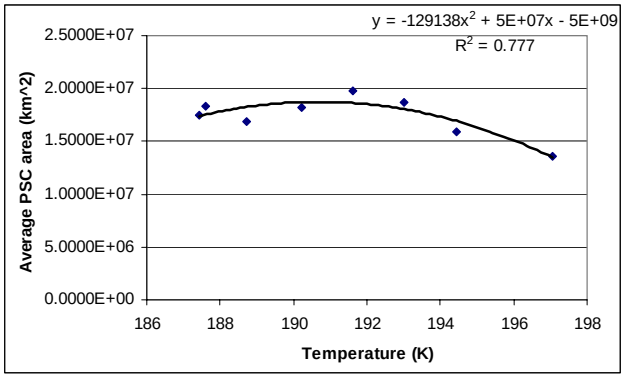

Figure 9: NAT formation temperature (K) vs. average PSC area (km^2) over the T_{NAT} period for 2005

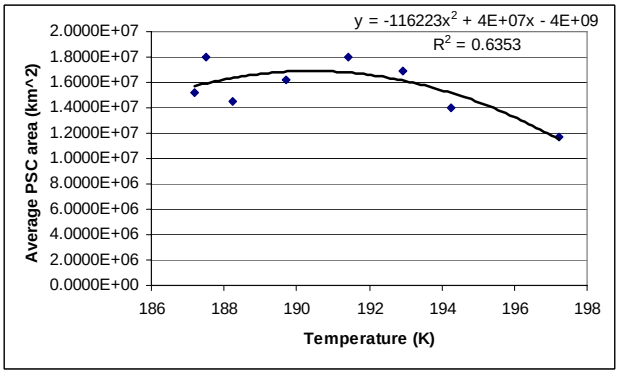

Figure 10: NAT formation temperature (K) vs. average PSC area (km^2) over the T_{NAT} period for 2006

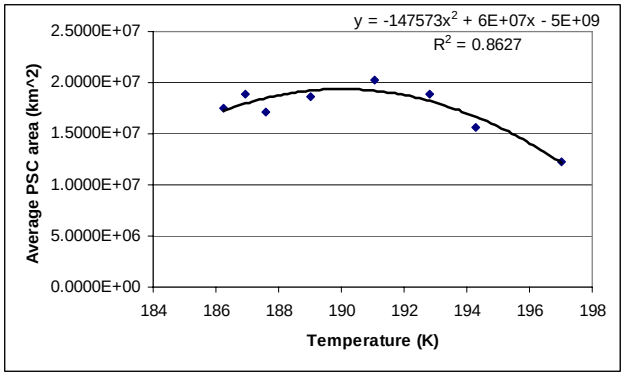

Figure 11: NAT formation temperature (K) vs. average PSC area (km^2) over the T_{NAT} period for 2007

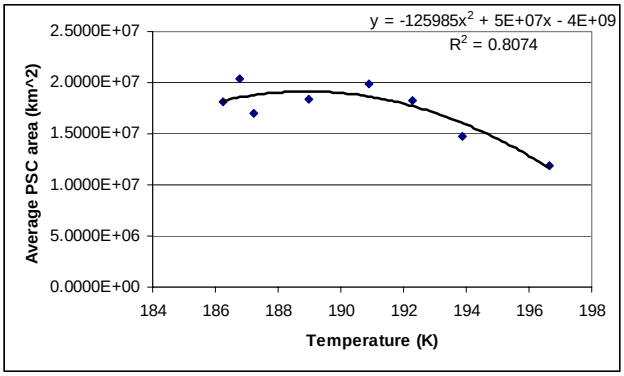

Figure 12: NAT formation temperature (K) vs. average PSC area (km^2) over the T_{NAT} period for 2008

3.3 Observed temperature vs. PSC area

Observed temperature was averaged over the two periods and plotted against PSC area for each year. This gave a strong linear relationship (average R^2 value of 0.83 and 0.72 for the AVP and T_{NAT} period respectively (see Figures 13 and 14). Although a squared polynomial fit showed a better R^2 for Figure 13 this would have used three fitting variables compared to two. Data over the T_{NAT} period showed most of the points were located along the left hand side of the graph.

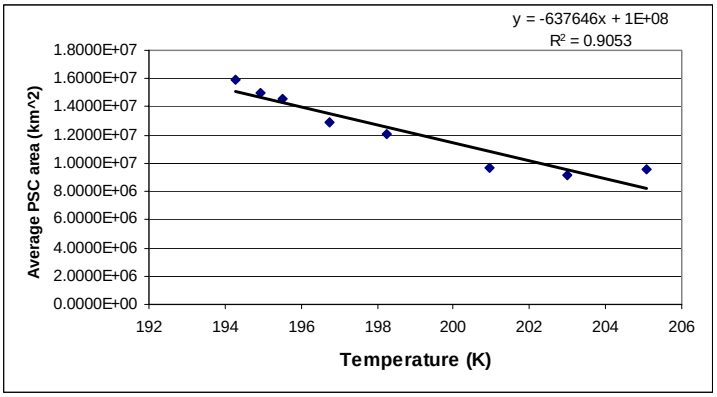

Figure 13: Observed average temperature (K) vs. average PSC area (km^2) over the AVP period for 2006

3.4 Temperature difference vs. PSC area

The difference between T_{NAT} and observed temperature was taken and plotted against average PSC area. A positive linear trend was only seen during the AVP, with an average R^2 value of 0.61. The strongest relationship was seen for 2006 (see Figure 15). No clear correlation was seen when the T_{NAT} period was averaged (see Figure 16). This comes as somewhat of a surprise as the temperatures during this period are always below $T_{NAT,}$ meaning PSCs can form, whereas half the AVP has temperatures above T_{NAT}. However we are using temperature averages over a vast area where half the true values are above and half below the average difference. This may explain the lack of a linear relationship.

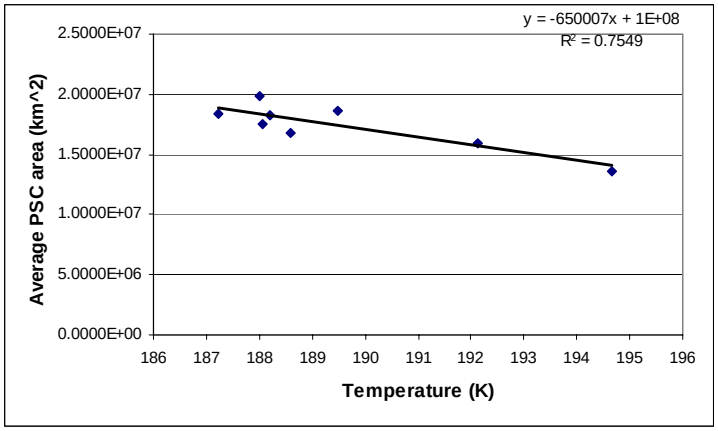

Figure 14: Observed average temperatures (K) vs. average PSC area (km^2) over the T_{NAT} period for 2005

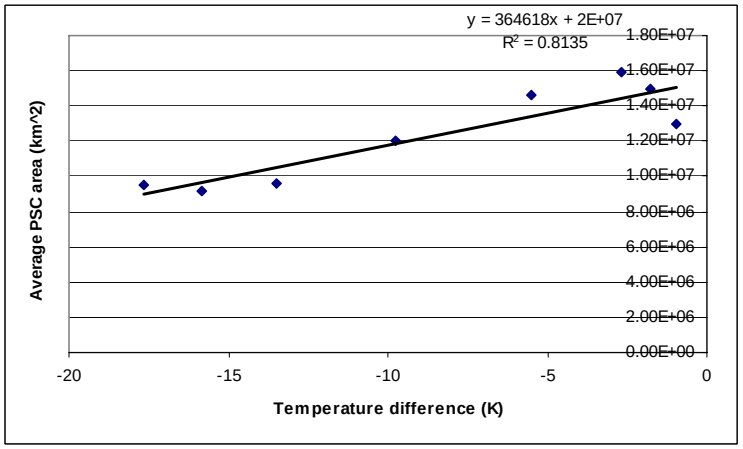

Figure 15: (T_{NAT} – observed temperature) vs. average PSC area (km^2) over the AVP period for 2006.

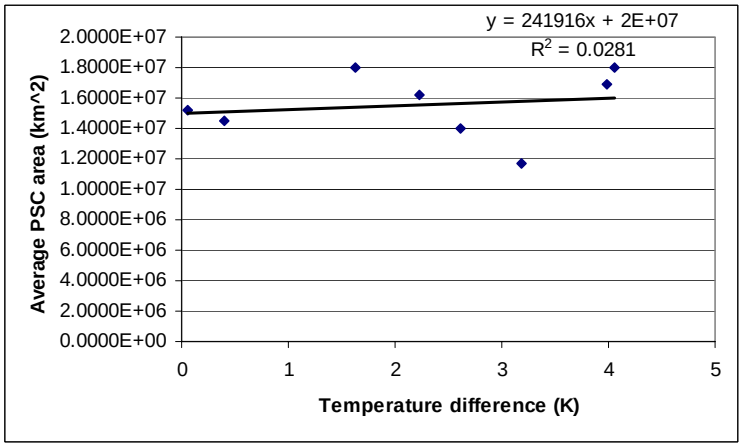

Figure 16: (T_{NAT} – observed temperature) vs. average PSC area (km^2) over the T_{NAT} period for 2006.

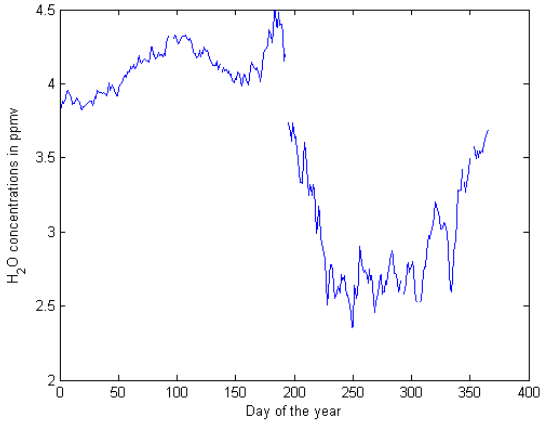

Figure 17: H_2O concentration (ppmv) for 2005 at pressure level 13

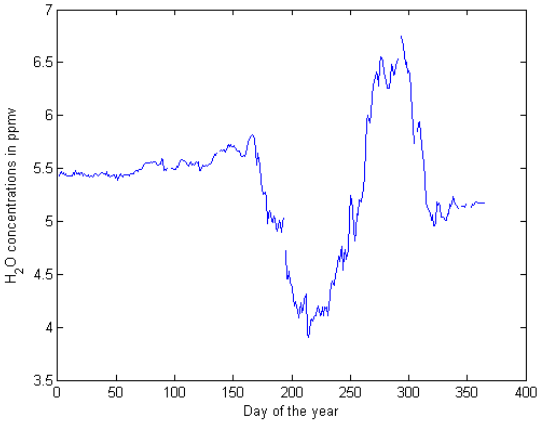

Figure 18: H_2O concentration (ppmv) for 2005 at pressure level 20

3.5 H_2O

A strong correlation between T_{NAT} and water vapour was observed, as discussed in section 3.1, Figure 3. Concentrations reach a maximum of 4.5 ppmv at pressure level 13 and rise to ~7 ppmv at pressure level 20 for 2005-2008 (see Figures 17 and 18 respectively). At pressure levels 13-19 a peak at day 170 is regularly observed before water levels being to drop as PSCs begin to form. This peak correlates well with values of T_{NAT} (Figure 3). Water levels drop about 1.5-2 ppmv for every level after this peak. These consistent patterns throughout altitude show that water behaviour does not considerably change in the first two thirds of the year. However as temperatures begin to rise again in mid August (day 220) water vapour patters begin to change with altitude. Levels increase in an unpredictable manner as the PSCs melt (see Figure 18). The strong rise and subsequent drop in water vapour in the upper pressure levels during days 210-310 is associated with atmospheric vertical motion. As illustrated in Figure 3 and Section 3.1 T_{NAT} is best explained by the water vapour patterns. However water vapour patterns also follow observed temperature, at least during the later parts of the year and for the lower pressure levels (see Figure 19).

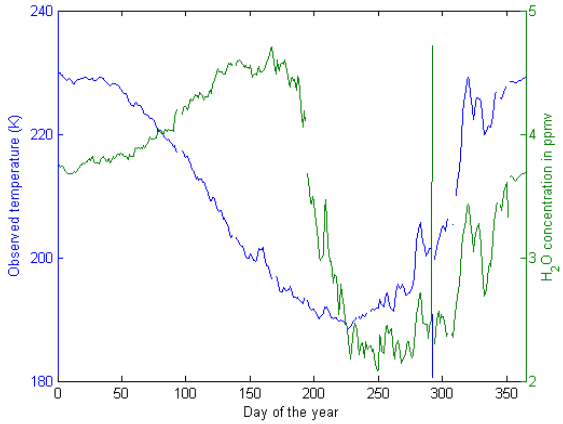

Figure 19: Observed temperature (K) and H2O concentration (ppmv) in 2005 at pressure level 14

No significant variability has been observed in the patterns between years.

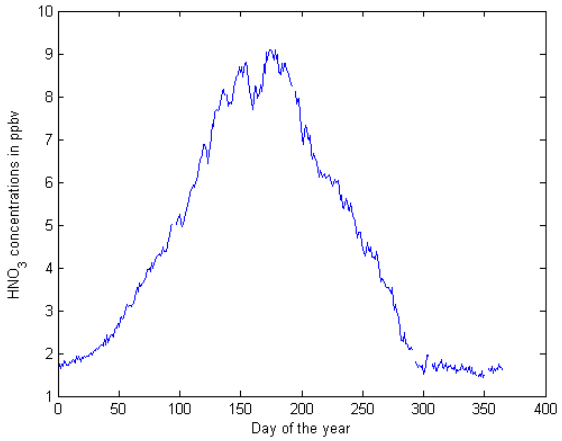

Figure 20: HNO_3 concentration (ppbv) for 2005 at pressure level 13

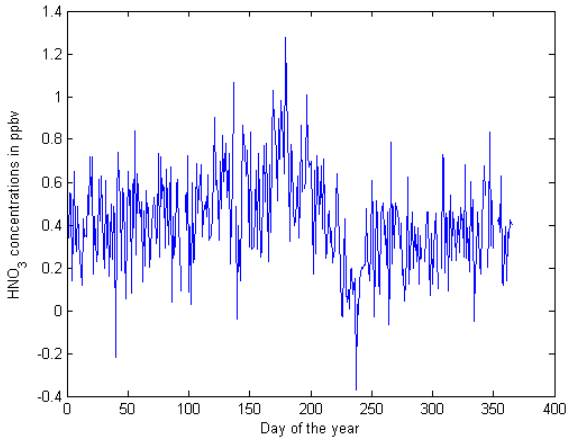

Figure 21: HNO_3 concentration (ppbv) for 2005 at pressure level 20

3.6 HNO_3

No strong correlation with the measured parameters other than the one mentioned for Figure 5 is seen for nitric acid. HNO_3 levels are in fact determine by levels of sunshine, or the lack thereof. As the days begin to shorten by day 50, HNO_3 levels rise to a maximum in mid winter during total darkness. As sunlight begins to return HNO_3 is removed as it reacts with the active chlorine species that are released. Concentrations reach a maximum of 7-9 ppbv depending on the year at pressure level 13, down to ~0.2ppbv at pressure level 20 (see Figures 20 and 21 respectively. After a continuous rise nitric acid concentrations begin to decrease at day 170, the time around which PSCs begin to form as T_{NAT} is reached. The decrease (denitrification) remains steady as nitric acid is incorporated into the NAT crystals, reaching a low of 1.5 ppbv at pressure level 13 and reaching 0 ppbv at pressure level 20. During November and December (days 300-365) levels remain steadily low as HNO_3 is released by the melting PSCs and mops up the chlorine. This phenomena has also been observed by Santee[3], who attributes this to the fact that the polar vortex has not yet collapsed, preventing HNO_3 rich mitlatitude air from helping remove the chlorine in the atmosphere. Santee also labels this event as denitrification. As the vortex fully collapses in January nitric acid levels begin to rise as they are replenished from the midlatitudes as well as melting PSCs. The MLS data analyzed by Santee showed HNO_3 levels equatorward of 65 degrees are indistinguishable, even in winter, for both hemispheres. Hence major denitrification

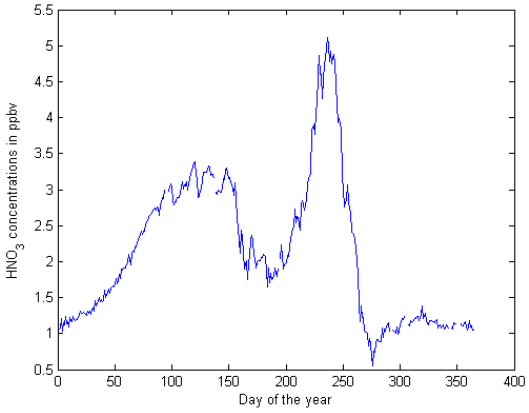

Figure 22: HNO_3 concentration in ppbv for 2005 at pressure level 14

only occurs below 65 degrees and has no strong influence on midlatitudes, and no long term influences at the poles are observed [3].

Pressure level 14 shows a unique trend that only occurs at this level for every year observed. HNO_3 levels rise with the onset of winter, but level off soon after, and drop in mid winter before rising again as the sunlight returns. This mid-winter drop must be associated with vertical air motion occurring within the polar vortex and only within this pressure zone, because if air motion occurred throughout the air column then one would expect a mid-winter disturbance in HNO_3 in all levels.

3.7 ClO

The pattern of ClO concentration in pressure levels 13-16 during the year most closely matches that of observed temperature (see Figure 23). ClO is removed completely by day 150 after a steady decline at the beginning of the year, and rises to a maximum level in early summer. The short increase and decrease starting at day 200 is an irregularity not seen in the other ClO graphs. Levels remain low and steady until around day 230 when observed temperatures start to increase along with ClO concentrations. During the darkness of winter ClO exists as the dimer Cl_2O_2 which decomposes into ClO when exposed to sunlight [14]. Sunlight begins to return to the edges of Antarctica around July, and day 230 is August 19th, by which time a significant area of the polar vortex is sunlit, creating a measurable increase in ClO as it forms from Cl_2O_2, alongside an increase in temperature. The depletion pattern seen in Figure 23 is similar for pressure levels 13-16 for every year, and ClO levels are reduced to near zero within those levels. However in the higher levels ClO removal is not complete, and values hover around the $1x10^{-4}$ ppmv mark (see Figure 24). Noise is quite high at high altitudes, but a trend of rises and falls can still be seen. Maximum levels of ClO do not change with altitude, remaining at around $3x10^{-4}$ ppmv throughout. This is in contrast to HNO_3 concentrations which experience a considerable decrease with increasing altitude. At level 17 the depletion pattern in Figure 23 begins to shift to the pattern observed in Figure 24. This new depletion pattern shows a maximum in late summer (day 100) rather than early summer, and shows an increase at day 170 rather than 230, at which point concentrations actually begin to decrease again. These patterns may be explained by the same mechanism

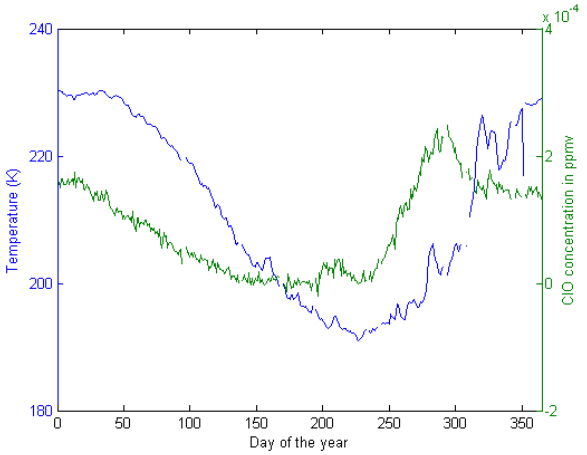

Figure 23: Observed temperature (blue, K) and ClO concentration (green, ppmv) for 2005 at pressure level 13

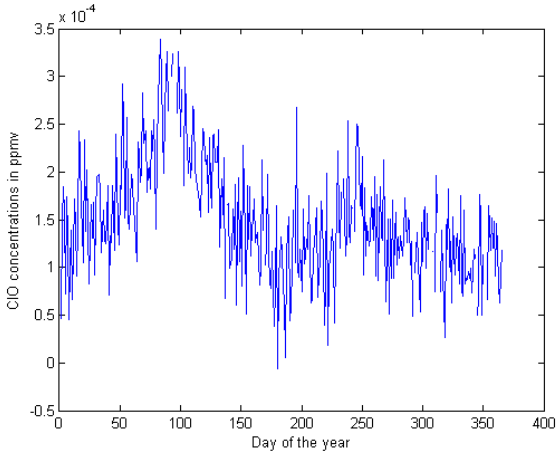

Figure 24: ClO concentration (ppmv) for 2005 at pressure level 20

responsible for the change in pattern of the other chemicals across altitude.

3.8 HCl

HCl depletion patterns in the lower pressure levels (13-15) most closely match up to the depletion patterns of water vapour (see Figure 25). This is in agreement with the observation that HCl depletion occurs in areas of high PSC density where you would expect to see a decrease in water vapour as PSCs form[15]. However the time of decrease in HCl is off by several months to that of the decrease in water vapour, which would indicate a different mechanism of HCl removal.

The depletion pattern starts to shift at level 16 to the one seen in Figure 26, where an increase in HCl concentration is seen at around the time when HCl depletion occurs in the lower pressure levels. HCl concentrations show an increase with increasing pressure level, with a maximum of 2.8×10^{-3} ppmv and a minimum of 2.3×10^{-3} ppmv for level 13, and a maximum of 3.7×10^{-3} ppmv and a minimum of 3.45×10^{-3} ppmv for level 20.

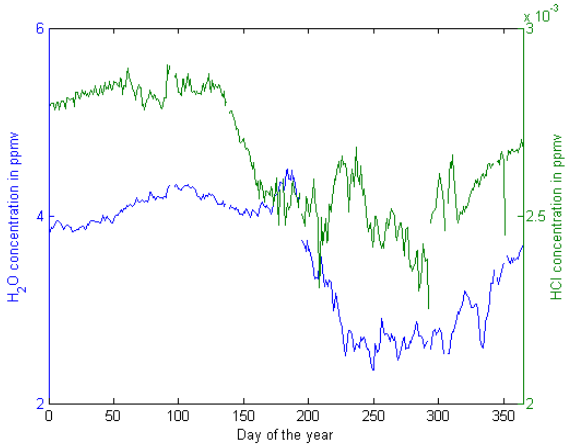

Figure 25: H_2O (blue) and HCl (green) concentration in ppmv for 2005 at pressure level 13

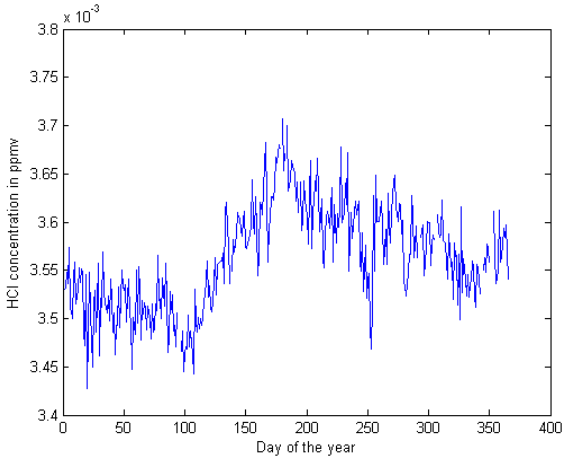

Figure 26: HCl concentration in ppmv for 2005 at pressure level 20

4 Discussion and Conclusion

There are several temperature relationships that have an effect on stratospheric behaviour and in turn an influence on PSC area, depending on which time periods that have been identified are studied. Initially temperatures that occur within the AVP were averaged and compared to PSC area, but it was soon realized that the period in which T_{NAT} is reached in the stratosphere did not coincide with the AVP. While the AVP officially lasts from the 18th of July to the 30th of November (day 199-333), a period of 134 days, temperatures below T_{NAT} were reached a month before, at around day 170 (mid-late May), and lasting for only 100 days. This gave us the opportunity to study two periods of the year that exhibit very different physical properties, and determine where the effects of temperature had the strongest effect.

Figures 6-12 showed the non-linear dependence of PSC area on T_{NAT} for both time periods. Squared polynomials with an average R^2 value of 0.92 were observed during the

AVP period, compared to an average R^2 value of 0.77 for the T_{NAT} period. Figures 13 and 14 showed a linear dependence of PSC on observed temperature during both time period, with an average R^2 value of 0.83 for observed temperature and an average R^2 value of 0.72 for the T_{NAT} period. This suggests observed temperature has a more direct influence on PSC formation than does T_{NAT}, and that the influence is more significant during the AVP period than during the T_{NAT} period. This conclusion is further supported by temperature differences plotted against PSC area (Figure 15). A less negative difference means observed temperatures were close to T_{NAT} and PSCs were more likely to form. However a large negative difference means temperatures were too warm for PSCs to form, leading to a smaller PSC area. This relationship was only observed during the AVP, and no relationship could be identified when using temperature data obtained during the T_{NAT} period. This trend may proof useful in applying temperature data from old records to back calculate the area of PSCs, and from this calculate levels of ozone depletion before satellite observations began.

Water vapour patterns during the years showed the regular appearance of a sudden spike in water concentrations at day 170 before they begin to drop. This rise can be attributed to adiabatic descent of water from the mesosphere, and could potentially offer a way of predicting the extent of ozone depletion for that year. This may be achieved by further investigation of the relative timing of the water vapour maximum.

A strong relationship was observed between T_{NAT} and water vapour as shown in Figure 3. As T_{NAT} is reached (dependant on water and HNO_3)PSCs begin to form, and water vapour is removed from the atmosphere. As water vapour pressures decrease PSCs are harder to form, requiring lower temperatures, and T_{NAT} decreases. As temperatures begin to warm some PSC crystals begin to melt, increasing the water vapour pressure and making it easier for PSCs to form again if temperatures fall again.

Water shows a trend of increasing concentration with increasing altitude, and different concentration patterns over the year for those different altitudes. This suggests there are several different altitude driven mechanisms acting on water throughout the year. In fact changes in concentration patterns across altitude are seen for all studied chemical species. Water vapour, ClO, and HCl all show an increase in concentration with increasing altitude, suggesting a similar mechanism is at work for all three species. HNO_3 shows a significant decrease in concentration with increasing altitude, due to a different mechanism, mainly that of being incorporated into NAT crystals as the limiting factor.

Of the four chemical species, HNO_3 shows the largest fluctuations in concentration across a year. Lower altitudes experience almost complete denitrification for at least several months during summer, and HNO_3 concentrations in higher altitudes are extremely low throughout the year. There, complete removal occurs during a few weeks over days 230 and 250. Because water concentrations remain comparatively high during the year HNO_3 is the limiting factor in NAT crystal formation, and very cold temperatures are required when HNO_3 levels are low. In fact T_{NAT} falls below 190K at pressure level 17 and above (Figure 2) from where maximum HNO_3 levels rapidly decrease from 5 ppbv to less than 1 ppbv. 190K is significantly lower than the standard 195K threshold used by many for their atmospheric calculations, but these low temperatures do occur at those heights, and PSCs can form. These upper altitudes contain water vapour and HNO_3 levels that can still create significant amounts of PSCs.

Therefore the 190K threshold should be taken into account in any ozone depletion models rather than using a constant value of 195K.

ClO and HCl concentrations are throughout the year very low, around $3x10^{-4}$ ppmv, or less than 1 ppbv, even lower than HNO_3. However these low concentrations can still be adequately observed via statellite. Their changes in concentration mainly depend on the presence of PSCs or sunlight, unlike water vapour and HNO3 where temperature is the deciding factor. Even at these low concentrations ClO and HCl a significant effect on ozone depletion due to their catalytic properties.

1. Schoeberl, M. R.; Hartmann, D. L., The dynamics of the stratospheric polar vortex and its relation to springtime ozone depletions. *Science* **1991,** 251, (4989), 46-52.
2. Solomon, S., Progress Towards a Quantitative Understanding of Antarctic Ozone Depletion *Nature* **1990,** 347, (6291), 347-354.
3. Santee, M. L.; Manney, G. L.; Froidevaux, L.; Read, W. G.; Waters, J. W., Six years of UARS Microwave Limb Sounder HNO3 observations:
Seasonal, interhemispheric, and interannual variations
in the lower stratosphere. *Journal of Geophysical Research* **1999,** 104 (D7), 8225-8246.
4. Lowe, D.; MacKenzie, A. R., Polar stratospheric cloud microphysics and chemistry. *Journal of Atmospheric and Solar-Terrestrial Physics* **2008,** 70, 13-40.
5. Hanson, D.; Mauersberger, K., Laboratory studies of the nitric acid trihydrate: Implications for the south polar stratosphere. *Geophysical Research Letters* **1988,** 15, (8), 855-858.
6. Peter, T., Microphysics and heterogeneous chemistry of polar stratospheric clouds. *Annual Review of Physical Chemistry* **1997,** 48, 785-822.
7. Carlsaw, K. S.; Luo, B. P.; Clegg, S. L.; Peter, T.; Brimblecombe, P.; Crutzen, P. J., Stratospheric aerosol growth and HNO_3 gas-phase depletion from coupled HNO_3 and water-uptake by liquid particles. *Geophysical Research Letters* **1994,** 21, 2479-2482.
8. Voigt, C.; Schlager, H.; Luo, B. P.; Dornbrack, A. D.; Roiger, A.; Stock, P.; Curtius, J.; Vossing, H.; Borrmann, S.; Davies, S.; Konopka, P.; Schiller, C.; Shur, G.; Peter, T., Nitric Acid Trihydrate (NAT) formation at low NAT supersaturation in Polar Stratospheric Clouds (PSCs). *Atmospheric Chemistry and Physics* **2005,** 5, 1371-1380.
9. Santee, M. L.; Tabazadeh, A.; Manney, G. L.; Salawitch, R. J.; Froidevaux, L.; Read, W. G.; Waters, J. W., UARS Microwave Limb Sounder HNO3 observations: Implications for Antarctic polar statospheric clouds. *Journal of Geophysical Research* **1998,** 103 (D11), 13,285-13,313.
10. Muscari, G.; Santee, M. L.; Zafra, R. L. d., Intercomparison of stratospheric HNO3 measurments over Antarctica: Ground-based millimeter-wave versus UARS/MLS Version 5 retrievals. *Journal of Geophysical Research* **2002,** 107(D24), 4809, doi: 10.1029/2002JD002546.
11. Livesey, N. J.; Read, W. G.; Froidevaux, L.; Waters, J. W.; Santee, M. L.; Pumphrey, H. C.; Wu, D. L.; Shippony, Z.; Jarnot, R. F., The UARS Microwave Limb Sounder version 5 data set: Theory, characterization, and validation. *Journal of Geophysical Research* **2003,** 108(D13), 4378, doi:10.1029/2002JD002273.
12. Huck, P. E.; McDonald, A. J.; Bodeker, G. E.; Struthers, H., Interannual variability in Antarctic ozone depletion controlled by planetary waves and polar

temperature. *Geophysical Research Letters* **2005,** 32 (L13819), doi:10.1029/2005GL022943.
13. Nedoluha, G. E.; Bevilacqua, R. M.; Fromm, M. D.; Hoppel, K. W.; Allen, D. R., POAM measurements of PSCs and water vapor in the 2002 Antarctic vortex. *Geophysical Research Letters* **2003,** 30, (15, 1796), doi:10.1029/2003GL017577.
14. Geller, M. A.; Yudin, V.; Douglass, A. R.; Waters, J. W.; Elson, L. S.; Roche, A. E.; III, J. M. R., UARS PSC, $ClONO_2$, HCl, and ClO measurements in early winter: Additional verification of the paradigm for chlorine activation. *Geophysical Research Letters* **1995,** 22, (21), 2937-2940.
15. Russell, J. M.; Gordley, L. L.; Park, J. H.; Drayson, S. R.; Hesketh, R. J.; Cicerone, A. F.; Frederick, J. E.; Harries, J. E.; Crutzen, P. J., The Halogen Occulation Experiment. *Journal of Geophysical Research* **1993,** 98, 10777-10797.
16. Hoppel, K.; Bavilacqua, R.; Allen, D. R.; Nedoluha, G. E.; Randall, C., POAM III observations of the anomalous 2002 Antarctic ozone hole. *Geophysical Research Letters* **2003,** 30, (7), 1394, doi:10.1029/2003GL016899.
17. Sinnhuber, B. M.; Weber, M.; Amankwah, A.; Burrows, J., Total ozone during the unusual Antarctic winter of 2002. *Geophysical Research Letters* **2003,** 30, (11), 1580, doi:10.1029/2002GL016798.